THE JOURNAL OF BIOLOGICAL CHEMISTRY
Vol. 280, No. 13, Issue of April 1, pp. 12917–12926, 2005
Printed in U.S.A.

Crystal Structures of Apo-form and Binary/Ternary Complexes of *Podophyllum* Secoisolariciresinol Dehydrogenase, an Enzyme Involved in Formation of Health-protecting and Plant Defense Lignans*

Received for publication, November 24, 2004, and in revised form, January 7, 2005
Published, JBC Papers in Press, January 13, 2005, DOI 10.1074/jbc.M413266200

Buhyun Youn‡, Syed G. A. Moinuddin§, Laurence B. Davin§, Norman G. Lewis§, and ChulHee Kang‡¶

From the ‡School of Molecular Biosciences, Washington State University, Pullman, Washington 99164-4660 and the §Institute of Biological Chemistry, Washington State University, Pullman, Washington 99164-6340

(−)-Matairesinol is a central biosynthetic intermediate to numerous 8–8′-lignans, including the antiviral agent podophyllotoxin in *Podophyllum* species and its semi-synthetic anticancer derivatives teniposide, etoposide, and Etopophos®. It is formed by action of an enantiospecific secoisolariciresinol dehydrogenase, an NAD(H)-dependent oxidoreductase that catalyzes the conversion of (−)-secoisolariciresinol. Matairesinol is also a plant-derived precursor of the cancer-preventative "mammalian" lignan or "phytoestrogen" enterolactone, formed in the gut following ingestion of high fiber dietary foodstuffs, for example. Additionally, secoisolariciresinol dehydrogenase is involved in pathways to important plant defense molecules, such as plicatic acid in the western red cedar (*Thuja plicata*) heartwood. To understand the molecular and enantiospecific basis of *Podophyllum* secoisolariciresinol dehydrogenase, crystal structures of the apo-form and binary/ternary complexes were determined at 1.6, 2.8, and 2.0 Å resolution, respectively. The enzyme is a homotetramer, consisting of an α/β single domain monomer containing seven parallel β-strands flanked by eight α-helices on both sides. Its overall monomeric structure is similar to that of NAD(H)-dependent short-chain dehydrogenases/reductases, with a conserved Asp^{47} forming a hydrogen bond with both hydroxyl groups of the adenine ribose of NAD(H), and thus specificity toward NAD(H) instead of NADP(H). The highly conserved catalytic triad (Ser^{153}, Tyr^{167}, and Lys^{171}) is adjacent to both NAD^+ and substrate molecules, where Tyr^{167} functions as a general base. Following analysis of high resolution structures of the apo-form and two complex forms, the molecular basis for both the enantio-specificity and the reaction mechanism of secoisolariciresinol dehydrogenase is discussed and compared with that of pinoresinol-lariciresinol reductase.

The 8–8′-linked lignans represent an abundant class of ubiquitous vascular plant natural products, with important roles in human health protection, pharmacological applications, as well as in plant defense (1, 2). Of these, the lignans matairesinol (**1**), secoisolariciresinol (**2**) (Fig. 1), or derivatives thereof can accumulate in high fiber foodstuffs and are metabolized in humans following dietary ingestion to afford the cancer-preventative "mammalian" lignans/"phytoestrogens" enterolactone (**3**) and enterodiol (**4**) (3, 4). Matairesinol (**1**) is also metabolized further in various vascular plant species, such as *Podophyllum*, to generate the antiviral podophyllotoxin (**5**) (5), with the latter being used as a starting material in the semi-synthetic preparation of the anti-cancer compounds teniposide (**6**), etoposide (**7**), and Etopophos® (**8**) (6). Additionally, matairesinol (**1**)-derived lignans can have important protective functions against various pathogenic organisms, *e.g.* as part of the chemical arsenal present in western red cedar heartwood (7–11).

From a biosynthetic pathway perspective, the studies on lignan-specific proteins and enzymes (2, 5, 10–31) have served to unambiguously distinguish further the biochemical pathways actually involved in both lignan and lignin formation. This directly contrasts with other reports (32–35) that have been interpreted to indicate that there is no control over phenoxy radical coupling, although it should be noted that some of these studies have already been retracted in part (35) and reinterpreted (36).

The biochemical pathway to (−)-matairesinol (**1a**) in *Podophyllum* and various other plant species begins with dirigent protein-mediated stereoselective coupling of two achiral molecules of *E*-coniferyl alcohol (**10**) to afford (+)-pinoresinol (**11a**) (Fig. 2) (13, 14, 23, 31). Dirigent proteins, which represent a new class of proteins (13, 14, 17), appear to be ubiquitous in the ferns, gymnosperms (24), and flowering angiosperms (14, 17, 18, 24) and may have evolved their functions during land plant evolution (17). In particular, the (+)-pinoresinol-forming dirigent protein has been extensively studied *in vitro* (23, 31), in terms of the kinetics of its unique stereoselective radical capture/coupling mechanism that controls both regio- and stereospecificities during phenoxy radical coupling.

Thus, a recent report (33) claiming that the (+)-pinoresinol-forming dirigent protein physiological function *in vivo* was "elusive" cannot be reconciled with the fact that its function has been explicitly and unambiguously documented *in vitro* (13, 23, 31), or that its patterns of gene expression *in vivo* are consistent with this function in numerous species (14, 17, 18, 24, 25). The generation of an "unnatural" lignan derived from 5-hydroxyconiferyl alcohol and coniferyl alcohol (**10**), in extracts

* This work was supported in part by NIGMS grants from the National Institutes of Health (to C. H. K. and N. G. L.), the United States Department of Agriculture Grant 99-35103-8037, McIntire-Stennis, and the Murdock Charitable Trust. The costs of publication of this article were defrayed in part by the payment of page charges. This article must therefore be hereby marked "*advertisement*" in accordance with 18 U.S.C. Section 1734 solely to indicate this fact.

The atomic coordinates and structure factors (code 2BGK, 2BGL, and 2BGM) have been deposited in the Protein Data Bank, Research Collaboratory for Structural Bioinformatics, Rutgers University, New Brunswick, NJ (http://www.rcsb.org/).

¶ To whom correspondence should be addressed: School of Molecular Biosciences, Washington State University, Pullman, WA 99164-4660. Tel.: 509-335-1409; Fax: 509-335-9688; E-mail: chkang@wsunix.wsu.edu.

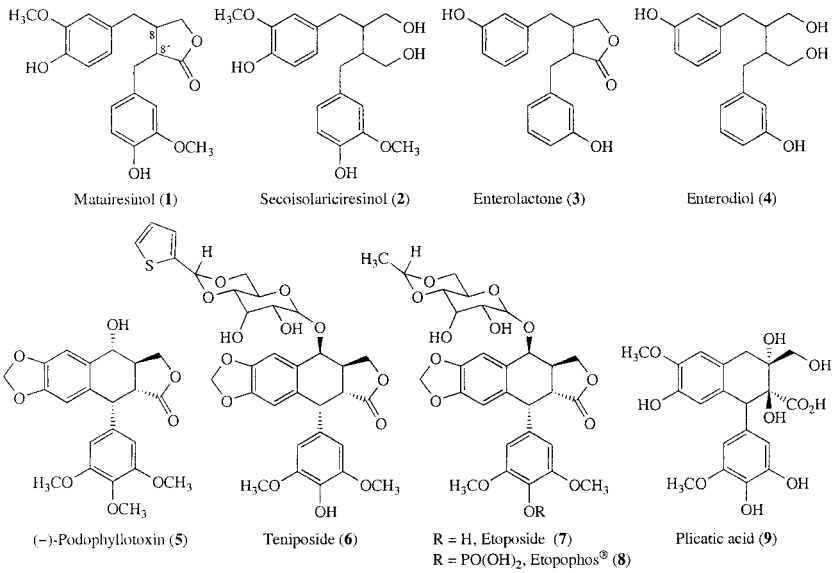

FIG. 1. **Selected examples of various 8–8′-linked lignans with roles in human health protection, pharmaceuticals, and plant defense.**

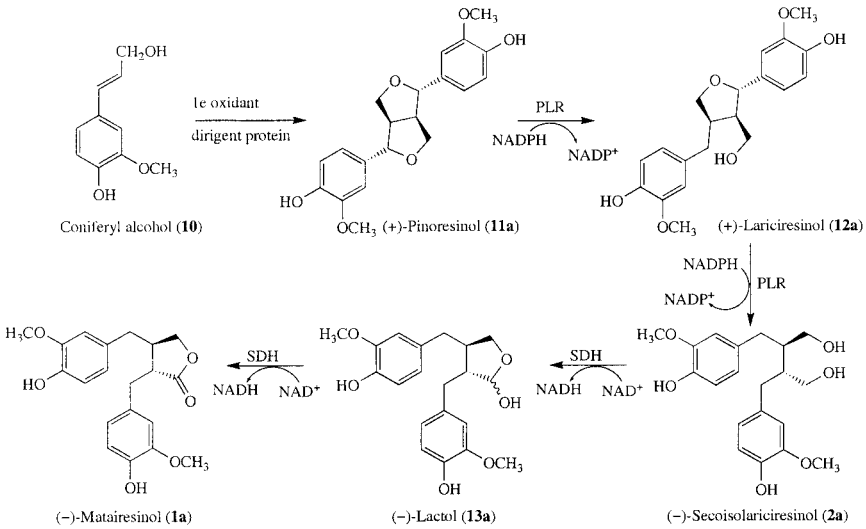

FIG. 2. **Biochemical pathway to (−)-matairesinol (1a) from *E*-coniferyl alcohol (10) in *Podophyllum* sp., where SDH catalyzes the enantiospecific conversion of (−)-secoisolariciresinol (2a) into (−)-matairesinol (1a) via intermediacy of (−)-lactol (13a).** Opposite enantiomers (structures not shown) are depicted in text as **1b**, **2b**, and **11b** to **13b**.

from caffeic acid *O*-methyltransferase-deficient poplar, is not evidence for the lack of stereoselective coupling control, because, for example, dirigent proteins have not been shown to bind and utilize 5-hydroxyconiferyl alcohol *in vitro*. Indeed, generation of this unnatural dimer is not unexpected given the experimental design employed. In contrast, there are innumerable examples of rigorous stereoselective and regiospecific coupling control in the plant kingdom involving formation of 8–8′-, 8–2′, 8–5′-, 8-*O*-4′-lignans, norlignans (1, 22, 26, 27, 29, 37, 38), ellagitannins (39, 40), etc. Such coupling systems can generate optically active, racemic, and optically inactive (regiospecific) coupling products, albeit through strict control of the coupling; these can be envisaged to utilize dirigent proteins or (oxidative) enzymes harboring dirigent sites.

Furthermore, in the case of (+)-pinoresinol (**11a**)-mediated formation in many species, the latter can undergo sequential enantiospecific reductions, catalyzed by the NADPH-dependent bifunctional pinoresinol-lariciresinol reductase (PLR)[1] (10, 12, 41), to afford initially (+)-lariciresinol (**12a**) and then (−)-secoisolariciresinol (**2a**). However, in certain other plant species, such as flax (*Linum usitatissimum*), the opposite stereoselective and enantiospecific transformations can predominate (16, 19, 20, 42), *i.e.* whereby (−)-pinoresinol (**11b**) is preferentially formed and then metabolized into (−)-lariciresinol (**12b**) and (+)-secoisolariciresinol (**2b**), respectively. There are also other examples, such as in *Thuja plicata*, where two enantiomerically distinct forms of PLR have been reported and fully characterized (1, 10, 11), and there is indirect evidence that different enantiospecific pathways in lignan biosynthetic pathways may be operative in distinct organs even within the same plant (43). These discoveries thus point again to the exquisite level of control exercised over phenoxy radical coupling processes and downstream metabolism.

More recently, it was possible to explain the molecular basis of catalysis and the distinct enantiospecificities of PLRs following comparative analyses of the x-ray crystal structure (2.5 Å resolution) of *T. plicata* PLR_Tp1 (10) and *L. usitatissimum* PLR_Lu (20) (with (−)-pinoresinol (**11b**)) and those catalyzing the opposite conversion using (+)-pinoresinol (**11a**), *i.e.* PLR_Tp2 (10) and *Forsythia intermedia* PLR_Fi1 (12). In all cases, a highly conserved Lys is required for general base catalysis as demonstrated by site-directed mutagenesis (K138A) through abolition of PLR_Tp1 catalytic activity (28). To account for the enantiospecific differences, a comparison of the amino acid sequences of PLR_Tp1/PLR_Lu and PLR_Fi1/PLR_Tp2, together with modeling of the PLR substrate binding

[1] The abbreviations used are: PLR, pinoresinol-lariciresinol reductase; Lu, *L. usitatissimum*; PDB, protein data bank; Pp, *P. peltatum*; r.m.s.d., root mean square deviation; SDH, secoisolariciresinol dehydrogenase; SDR, short-chain dehydrogenases/reductases; Tp, *T. plicata*.

pocket, revealed symmetrical substitutions in both enantiospecific classes favoring binding of the (−)-antipode (**11b**) with PLR_Tp1/PLR_Lu and (+)-pinoresinol (**11a**) with PLR_Tp2/PLR_Fi1, *i.e.* from Val^{268}/Leu^{272} in PLR_Tp1 (Val^{265}/Leu^{272} in PLR_Lu) to Gly^{267}/Phe^{271} in PLR_Tp2 (Gly^{268}/Tyr^{272} in PLR_Fi1), respectively. A third amino acid substitution, in the enantiospecifically distinct PLR_Tp1 and PLR_Tp2, was also considered as potentially enhancing substrate binding specificity in *Thuja* species, *i.e.* from Phe^{164} in PLR_Tp1 to Leu^{164} in PLR_Tp2 (28). Although there were other symmetrical substitutions in both PLR enantiospecific classes (*i.e.* those at the equivalent positions of Gln^{47}, Leu^{128}, Gln^{252}, and Met^{305} in PLR_Tp1), these are more likely associated with substrate access or gating rather than being involved in binding/catalysis.

The current study was therefore next directed toward establishing the crystal structure of secoisolariciresinol dehydrogenase (SDH), which catalyzes the enantiospecific conversion of (−)-secoisolariciresinol (**2a**) into (−)-matairesinol (**1a**) (Fig. 2) (5, 21). This is the last enzymatic step in vascular plants to the precursor of the mammalian lignan, enterolactone (**3**), as well as being involved in the pathway to the antiviral lignan, podophyllotoxin (**5**), and thus to its semi-synthetic derivatives, teniposide (**6**), etoposide (**7**), and Etopophos® (**8**). As indicated earlier, it is also an obligatory step to various plant defense metabolites, such as plicatic acid (**9**).

EXPERIMENTAL PROCEDURES

Metabolite Isolation—(−)-Matairesinol (**1a**) was isolated from *F. intermedia* stems as described in Umezawa *et al.* (44).

Expression and Purification of SDH—SDH_Pp7, cloned into an Invitrogen pTrcHis2-TOPO® TA vector, was transformed into TOP10 *Escherichia coli* cells as described previously (21). Expression of SDH_Pp7 was induced by addition of isopropyl β-D-thiogalactopyranoside to 1 mM final concentration at mid-log phase (A_{600} = 0.5–0.7). The induced cell suspension cultures were grown for 12 h at 37 °C, with shaking at 250 rpm. The cells were then harvested by centrifugation (3,000 × *g* for 20 min). The SDH_Pp7-derived pellet was suspended in Buffer A (20 mM Tris-HCl (pH 8.0) containing EDTA (3 mM) and dithiothreitol (3 mM)), sonicated (5 × 10 s, model 450 sonifier®, Branson Ultrasonics Co.), and centrifuged (20,000 × *g* for 40 min). The resulting supernatant was next subjected to ammonium sulfate precipitation, with the recombinant SDH_Pp7 precipitating between 70 and 80% ammonium sulfate. This fraction was reconstituted in 40 ml of Buffer A, desalted over a PD-10 column (Amersham Biosciences), then subjected to anion exchange column chromatography (Self Pack™ POROS® 10HQ, Applied Biosystems) pre-equilibrated in Buffer B (50 mM Tris-HCl (pH 7.5) containing EDTA (3 mM) and dithiothreitol (1 mM)), at a flow rate of 5 ml min^{-1}. Recombinant SDH_Pp7 was eluted using a NaCl step gradient (to 0.1, 0.2, 0.5, and 2.0 M, 50 ml each), and the corresponding fractions of interest (eluting at 0.1 M NaCl) were desalted and concentrated into Buffer B by ultrafiltration in an Amicon 8050 cell with a 10-kDa cut-off membrane (Millipore). The concentrated SDH_Pp7 was next applied to a MonoQ® HR16/10 (Amersham Biosciences) anion exchange column equilibrated in Buffer B at a flow rate of 3 ml min^{-1} and eluted using a NaCl step gradient (to 0.05, 0.1, 0.2, 0.4, and 2.0 M; 20 ml each); the corresponding catalytically active fractions were eluted at 0.05 M NaCl. This SDH_Pp7-enriched fraction was then concentrated as above, the buffer exchanged to 5 mM sodium phosphate (pH 6.8), and applied to a CHT-10 hydroxyapatite (Bio-Rad) column (1 × 10 cm), equilibrated in the same buffer, at a flow rate of 3.5 ml min^{-1}. The column was eluted with a linear sodium phosphate gradient (5–500 mM in 200 ml). SDH_Pp7 did not bind to the matrix, and the flow-through fraction containing it was concentrated as above with the buffer exchanged to Buffer B. The resulting SDH_Pp7-enriched protein fraction was then applied to a MonoQ™ GL10/100 anion exchange column (Amersham Biosciences) equilibrated in Buffer B at a flow rate of 2 ml min^{-1} and eluted with a NaCl step gradient (0.05, 0.1, 0.2, 0.4, and 2.0 M; 20 ml each); the catalytically active SDH_Pp7 fraction eluted at 0.05 M NaCl. The SDH_Pp7 so obtained was concentrated, with a final purity >99% as estimated by SDS-PAGE (Coomassie Blue staining).

Molecular Mass Determination by Size Exclusion Chromatography and Multiangle Laser Light Scattering—A TSK G3000SW (TosoHaas) column was pre-equilibrated in Buffer B followed by loading of the SDH_Pp7 solution (100 μl, 1 or 2 mg ml^{-1}) in the same buffer. The chromatography was performed at a flow rate of 1 ml min^{-1} and a temperature of 22 °C by using an Acuflow series IV pump (Analytical Instruments), with the resulting eluant passed in tandem through a UV detector (Gilson), a refractometer (Optilab DSP, Wyatt Technology Corp.), and a multiangle laser light-scattering detector (Dawn EOS, Wyatt Technology Corp.), respectively, with the scattering data analyzed using the software ASTRA (Wyatt Technology Corp.). Relative weight-average molecular masses were determined from the scattering data using the Zimm fitting method, in which $K^*c/R(Q)$ is plotted against $sin^2(Q/2)$, where Q is the scattering angle; $R(Q)$ is the excess intensity (I) of scattered light at the angle Q; c is the concentration of the sample, and K^* is a constant equal to $4\pi^2n^2(dn/dc)^2/\lambda_0{}^4N_A$ (where n = solvent refractive index; dn/dc = refractive index increment of scattering sample; λ_0 = wavelength of scattered light, and N_A = Avogadro's number). Extrapolation of the Zimm plot to zero angle gave an estimate of the weight-averaged molecular mass ($\bar{M}_w$), where the latter is defined in Equation 1,

$$\bar{M}_w = \frac{\sum(ciMi)}{\sum ci} \qquad \text{(Eq. 1)}$$

for c moles of i different species with individual molecular weights (Mi).

Crystallization of SDH_Pp7—For crystallization of the apo-form and complex forms, a solution of purified SDH_Pp7 (52 mg ml^{-1}) in 20 mM Tris-HCl (pH 8.0) containing 1 mM EDTA and 1 mM dithiothreitol was prepared. Crystallization trials were performed using the hanging drop vapor diffusion method at two temperatures (277 and 293 K). Apo-SDH_Pp7 crystals were obtained by mixing the above protein solution (1.5 μl) with an equal volume of reservoir solution containing 30% (w/v) PEG 4000, 0.1 M Tris-HCl (pH 8.5) and 0.2 M sodium acetate trihydrate. Diffraction quality crystals usually appeared after 10 days, and larger crystals with dimensions of ~0.3 × 0.4 × 0.7 mm were obtained after 2 weeks. The crystal of apo-SDH belongs to the orthorhombic space group, $C222_1$ (a = 107.34, b = 133.56, c = 69.35 Å), with two molecules in the asymmetric unit. The binary complex (SDH_Pp7-NAD^+) and the ternary complex (SDH_Pp7-NAD^+-(−)-matairesinol (**1a**)) crystals were also produced under the same conditions except for addition of 10 mM NAD^+ and 5 mM NAD^+, 2 mM (−)-matairesinol (**1a**), respectively. Both binary and ternary complexes crystallized in an orthorhombic space group, F222, with corresponding unit cells of a = 58.51, b = 118.91, c = 132.00 Å and a = 57.35, b = 118.74, c = 131.25 Å, respectively. The apo-form (1.6 Å resolution), the binary complex (2.8 Å), and the ternary complex (2.0 Å) data were collected from the Berkeley Advanced Light Source (ALS, beam line 8.2.1), Rigaku R-AXIS IV^{++}/RU H2R and Rigaku Saturn 92/FR-E, respectively, at a temperature of 100 K.

Structural Solution and Refinement—The structure of apo-SDH_Pp7 was solved by the molecular replacement method using a coordinate of the Rv2002 Gene Product from *Mycobacterium tuberculosis* (PDB 1NFF) (45) and the software package AmoRe (46). The rigid body refinement of the initial position was carried out by using 15.0 to 3.0 Å resolution data and gave an R value of 42%. After several cycles of positional and temperature factor refinements using the program X-PLOR (47) and a series of simulated annealing omit maps, most residues were fitted against the electron density, although the electron density corresponding to 10 N-terminal residues was not visible from an early stage of refinement. The binary and ternary complexes of SDH_Pp7 were again solved by the molecular replacement method but now using the apo-SDH_Pp7 coordinates. The final R factors (Table I) for the apo-form, as well as the binary and ternary complexes of SDH_Pp7, were 19.7% (R_{free} = 22.6% for the random 5% data), 20.1% (R_{free} = 22.1% for the random 5% data), and 20.0% (R_{free} = 22.9% for the random 5% data), respectively. The number of reflections above 2σ level for the apo-form were 63,119 (99.7% completeness) between 10.0- and 1.6-Å resolution. The crystals of the binary and ternary complexes did not diffract as well as the apo-form and gave reflection numbers of 4,585 (above 2σ, 99.7% completeness) between 10.0 and 2.8 Å resolution and 11,716 (above 2σ, 79.1% completeness) between 10.0 and 2.0 Å resolution. The root mean square deviations (r.m.s.d.) (from ideal geometry) of the final coordinates corresponding to apo-form and binary/ternary complexes are 0.01, 0.01, and 0.02 Å for bonds and 2.7, 3.2, and 3.3° for angles, respectively. All SDH_Pp7 coordinates have been deposited in the Protein Data Bank with codes 2BGK (apo-form), 2BGL (binary complex) and 2BGM (ternary complex).

TABLE I
Crystallographic data for the SDH-Pp7 apo, binary and ternary complex forms

	Apo	Binary[a]	Ternary[b]
Data			
Wavelength (Å)	1.0332	1.54	1.54
Resolution (Å)	50 to1.6	50 to 2.8	50 to 2.0
Space group	$C222_1$	F222	F222
Cell dimensions (Å)	a = 107.34 b = 133.56 c = 69.35	a = 58.51 b = 118.91 c = 132.00	a = 57.35 b = 118.74 c = 131.25
Asymmetric unit	2 molecules	1 molecule	1 molecule
Total observations	259,713	20,597	70,809
Unique reflections	93,528	5,752	12,187
Completeness (%)	99.7	99.7	79.1
R_{sym}[c,d]	4.0 (13.6)	5.7 (11.4)	5.0 (12.6)
Refinement			
Resolution (Å)	10 to 1.6	10 to 2.8	10 to 2.0
No. of reflections	63,119	4,585	11,716
R_{cryst}[e]	19.7	20.1	20.0
R_{free}[f]	22.6	22.1	22.9
r.m.s.d. bonds (Å)	0.01	0.01	0.02
r.m.s.d. angles (°)	2.7	3.2	3.3
No. of atoms			
Protein and ligand	3972	2030	2056
Water	288	28	127

[a] SDH_Pp + NAD^+.
[b] SDH_Pp7 + NAD^+ + (−)-matairesinol (**1a**).
[c] Numbers in parentheses refer to the highest resolution shell.
[d] $R_{sym} = \Sigma|I_h - \langle I_h\rangle|/\Sigma I_h$, where $\langle I_h\rangle$ is the average intensity over symmetry equivalent reflections.
[e] $R_{cryst} = \Sigma|F_{obs} - F_{calc}|/\Sigma F_{obs}$, where summation is over the data used for refinement.
[f] R_{free} was calculated as for R_{cryst} by using 5% of the data that was excluded from refinement.

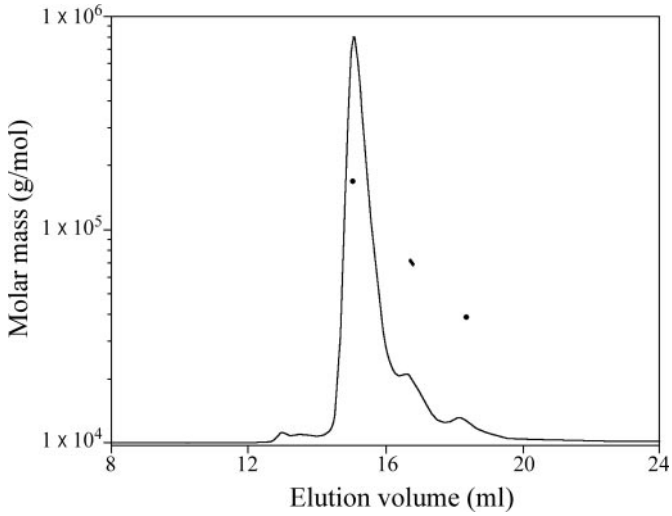

FIG. 3. **Multiangle laser light-scattering elution profile of SDH_Pp7 revealing tetrameric status.** Elution profiles are shown as molecular weight *versus* elution volume. The *solid lines* represent changes in refractive index on an arbitrary scale that is proportional to protein concentration. *Dots* indicate calculated molecular masses. For elution details, see "Experimental Procedures."

RESULTS AND DISCUSSION

Overall Structures—Recombinant *Podophyllum peltatum* secoisolariciresinol dehydrogenase (SDH_Pp7) was crystallized in its apo-, binary and ternary complex forms, with crystals of the latter two complexes obtained by mixing SDH_Pp7 with NAD^+ and NAD^+/(−)-matairesinol (**1a**), respectively, instead of diffusing ligands into the crystals; (−)-matairesinol (**1a**) was isolated from *F. intermedia* as described previously (44).

The structure of the apo-form of SDH_Pp7 was determined at 1.6 Å resolution by molecular replacement using coordinates of the Rv2002 Gene Product from *M. tuberculosis* (PDB 1NFF), which has the highest sequence similarity to SDH_Pp7 of sequences in the PDB (45). In turn, the binary and ternary complex structures of SDH_Pp7 were determined at 2.8 and 2.0 Å resolution, respectively, using the coordinates of the deduced apo-form SDH_Pp7 structure. The apo-form was found to have two tightly associated molecules in its asymmetric unit, and a crystallographic symmetry operation assembled these two molecules into a tetrameric unit in the crystal lattice; both molecules in an asymmetric unit were virtually superimposable with an r.m.s.d. of 0.87 Å between the corresponding C-α carbons. Additionally, the oligomeric status of SDH_Pp7 as a tetramer was verified in solution by a multiangle laser light-scattering experiment, *i.e.* analyses of solutions of purified SDH_Pp7 (1 and 2 mg ml^{-1}, respectively) revealed that it was mainly of intrinsic tetramer character (Fig. 3). A different crystal form of the P1 space group was also obtained, which contained the same type of tetramer as the asymmetric unit, but this was not examined further because the corresponding diffraction data were of relatively low resolution (~3.0 Å).

The SDH_Pp7 monomer contains a single α/β domain structure with a characteristic NAD(H)-binding motif (Fig. 4*A*), which consists of seven parallel β-strands (βA–βG) with both sides surrounded by eight α-helices (αA–αH). These connect the strands like those typically observed in the Rossmann fold, *i.e.* for proteins having NAD(P)H- and FMN-binding signatures, such as oxidoreductases and transferases. In particular, there are two α-helices (αF and αG) between the 6th and the 7th β-strand (βF and βG) establishing its overall topology of $\beta\alpha\beta\alpha\beta\alpha\beta\alpha\beta\alpha\beta\alpha\alpha\beta\alpha$. Furthermore, because this topology also showed a close resemblance to those of short-chain dehydrogenases/reductases (SDR), a detailed comparison using a Dali search (48) was carried out to identify structural homologues. The highest match was to the 3-hydroxyacyl-CoA dehydrogenase from rat brain (PDB 1E6W) with a *Z*-score of 32.0; this was followed by a 3-α,20-β-hydroxysteroid dehydrogenase from *Streptomyces exfoliatus* (PDB 2HSD) with a *Z*-score of 31.8 and a glucose dehydrogenase from *Bacillus megaterium* (PDB 1GCO) of 29.1. On the other hand, an amino acid sequence analysis (49) of the PDB revealed that the Rv2002 gene product from *M. tuberculosis* (1NFF) shows the highest similarity (33.8%) to SDH_Pp7, followed by the 3-α,20-β-hydroxysteroid dehydrogenase from *S. exfoliatus* (PDB 2HSD; 31.8%), an *R*-specific alcohol dehydrogenase from *Lactobacillus brevis* (PDB 1NXQ; 30%), and the rat brain 3-hydroxyacyl-CoA dehydrogenase described above (PDB 1E6W; 27.4%) (Fig. 5). In terms of overall topology of the secondary structural elements, however, the 3-α,20-β-hydroxysteroid dehydrogenase from *S. exfoliatus* (PDB 2HSD) is most similar to that observed in the structure of SDH_Pp7, although the location and size of the αE was rather different in both structures.

Furthermore, the sequence alignment of the various dehydrogenases and reductases (Fig. 5) revealed that they have several deletions and insertions when compared with SDH_Pp7, with some missing the αH region. In particular, the highly disordered region containing 10 N-terminal amino acids in SDH_Pp7 cannot be aligned relative to the above listed dehydrogenases and reductases. The longest region of highest sequence similarity between SDH_Pp7 and the various SDRs is the area between Glu^{234} and Gly^{261}, which spans most of the αG and βG region. Significantly, the level of sequence similarity among the various SDRs is very low in the region between residues Leu^{205} and Ala^{233}, and this region also happens to contain a major insertion site in SDH_Pp7. This inserted area spans the αF, including its N- and C-flanking loops, and is involved in an intermolecular helix-helix interaction with the αH of another molecule, thereby forming the substrate-binding pocket. Additionally, the loop area connecting the βE and αE

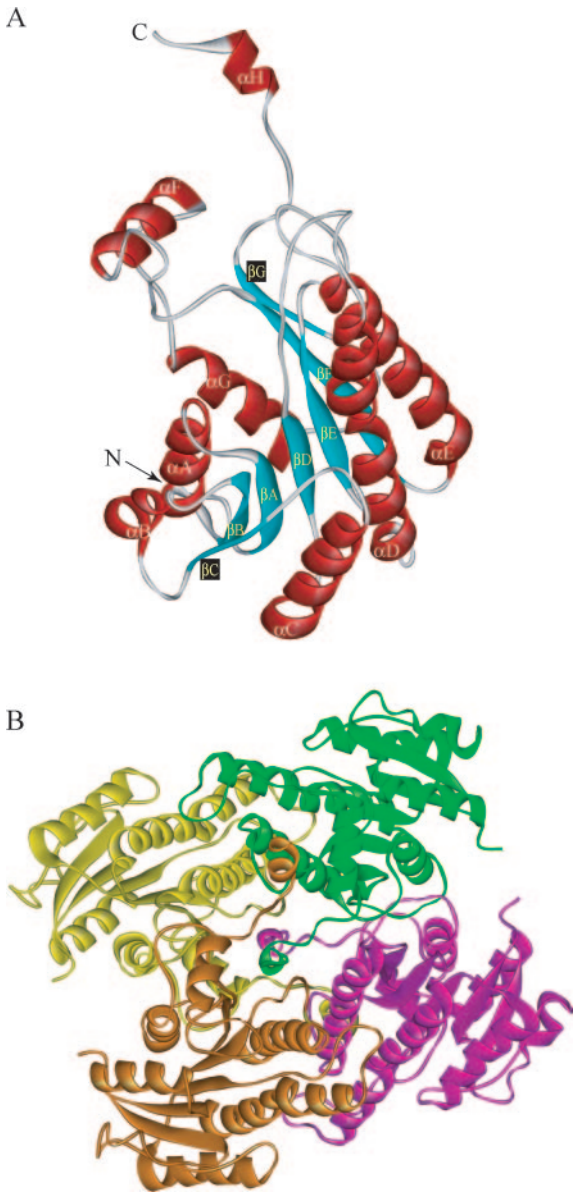

FIG. 4. **Crystal structures of SDH_Pp7.** *A*, structural element distribution of the monomeric form. Secondary structure elements have been numbered sequentially as αA–αH and βA–βG for the common helices and strands, respectively. *N* and *C* refer to N- and C-terminal regions, respectively. *B*, arrangement of the tetrameric SDH_Pp7 in a D_2 symmetry. The pairs of *yellow* and *brown* molecules (or *green* and *fushia*) are related by the pseudo 2-fold axis, which becomes a crystallographic 2-fold axis in both binary and ternary complex crystals.

regions displays a low level of sequence similarity, and some of the residues in this loop are in close contact with the substrate, such as Ile^{154}, Ser^{155}, and Ser^{156}. Indeed, these observations are in agreement with a previous finding that some of the unique insertions or local heterogeneities for each SDR are to support the binding of their specific substrates (50).

In terms of the substrate binding pocket and the catalytic mechanism, all of these enzymes have a conserved catalytic triad containing Tyr, Lys, and Ser (51). In SDH_Pp7, the Tyr^{167} and Lys^{171} are located near the carboxyl end of the αE, whereas Ser^{153} is located in the loop connecting both the αE and βE regions. In its apo-form, the hydroxyl group of Ser^{153} is hydrogen-bonded to the phenolic group of Tyr^{167}, with the protonated amino group of Lys^{171} being located ~4.0 Å from the Tyr^{167} phenolic group (Fig. 6*A*, *inset*).

Finally, in addition to the highly disordered N-terminal amino acids, three other areas show either partial disorder or higher temperature factors than the rest of the SDH_Pp7 molecule (Fig. 7), *i.e.* residues 48–61, which are around the αB region exposed to the surface, and residues 201–215 and 272–277. As clearly shown in Fig. 7, the area of residues 48–61 shows significantly reduced temperature factors upon complex formation reflecting its relationship with cofactor binding as discussed later. The other two areas of residues 201–215 and 272–277 are the least conserved regions among various SDRs and alcohol dehydrogenases (Fig. 5). In particular, residues 200–218 are part of the above-mentioned inserted αF area that is in close proximity to the substrate-binding pocket and probably determine a unique specificity for (−)-secoisolariciresinol (**2a**); this local area also shows the largest conformational difference among the apo-form and binary and ternary complexes as discussed later.

Tetramer Formation—The individual subunits of SDH_Pp7 are arranged around two intersecting 2-fold axes forming a D_2 symmetry among the four subunits (Fig. 4*B*), thereby stabilizing the tetramer through tight intermolecular interactions among the four molecules. In the apo-form, the two monomers are in an asymmetric unit, related by the noncrystallographic 2-fold axis, and show a strong intermolecular interaction via a four-helix bundle motif formed by two αD and two αE regions (between *violet* and *brown, yellow* and *green* in Fig. 4*B*). Accordingly, this monomer-monomer interface is mainly stabilized by a large number of hydrophobic interactions between the αD helices and the six side-chain hydrogen bonds between the αE helices. In both the binary and ternary complexes, however, this pseudo 2-fold axis becomes a crystallographic 2-fold axis. The second type of dimer that is related to the crystallographic 2-fold axis in both apo- and complex forms of SDH_Pp7 is also stabilized via hydrogen bonding and hydrophobic interactions, especially between the αH of one subunit and αF of the other (between *violet* and *green, yellow* and *brown* in Fig. 4*B*). This exchange interaction of the αH between monomers is comparable with a domain swapping or an arm exchange. In particular, the 10 C-terminal residues of one SDH_Pp7 monomer become inserted into a relatively hydrophobic cleft of the other, thereby forming two intermolecular hydrogen bonds. Furthermore, near the point where the C-terminal arm leaves each monomer, there is a Pro^{267}, *i.e.* a typical proline residue found in hinge regions of other domain swapping systems.

Overall, however, there are no major conformational differences in the backbone structures among the apo-form and the binary and the ternary complexes (Fig. 8*A*), except for the area of residues 201–222 and C-terminal residues 273–277 (*boxed areas* in Fig. 8*A*). Furthermore, the C-α carbons of the binary and ternary complexes are superimposable with an r.m.s.d. of 0.71 Å; the apo-form can also be made superimposable with the binary and ternary complexes of 1.22 and 1.08 Å, respectively, showing somewhat larger changes than between the binary and ternary complexes.

Cofactor Binding—The electron density corresponding to NAD^+ was clearly identifiable from the initial $F_o - F_c$ map (Fig. 9*A*). In the apo-form, this cofactor-binding site is filled with water molecules, thereby forming a hydrogen bond network (Fig. 6*A*, *inset*) with the side chains of the lined residues, particularly that of the highly conserved catalytic triad, Ser^{153}, Tyr^{167}, and Lys^{171} (Fig. 6*A*). As can be seen, the nicotinamide ring assumes a *syn*-conformation, whereas the adenine ring has an *anti*-conformation (Fig. 6*B*). As in other NAD(P)H-dependent oxidoreductases, the carboxyl ends of βA, βB, βD, βE, βF, and the loop connecting βF and αF also form a cleft for cofactor binding. In this position, the nicotinamide is stabilized

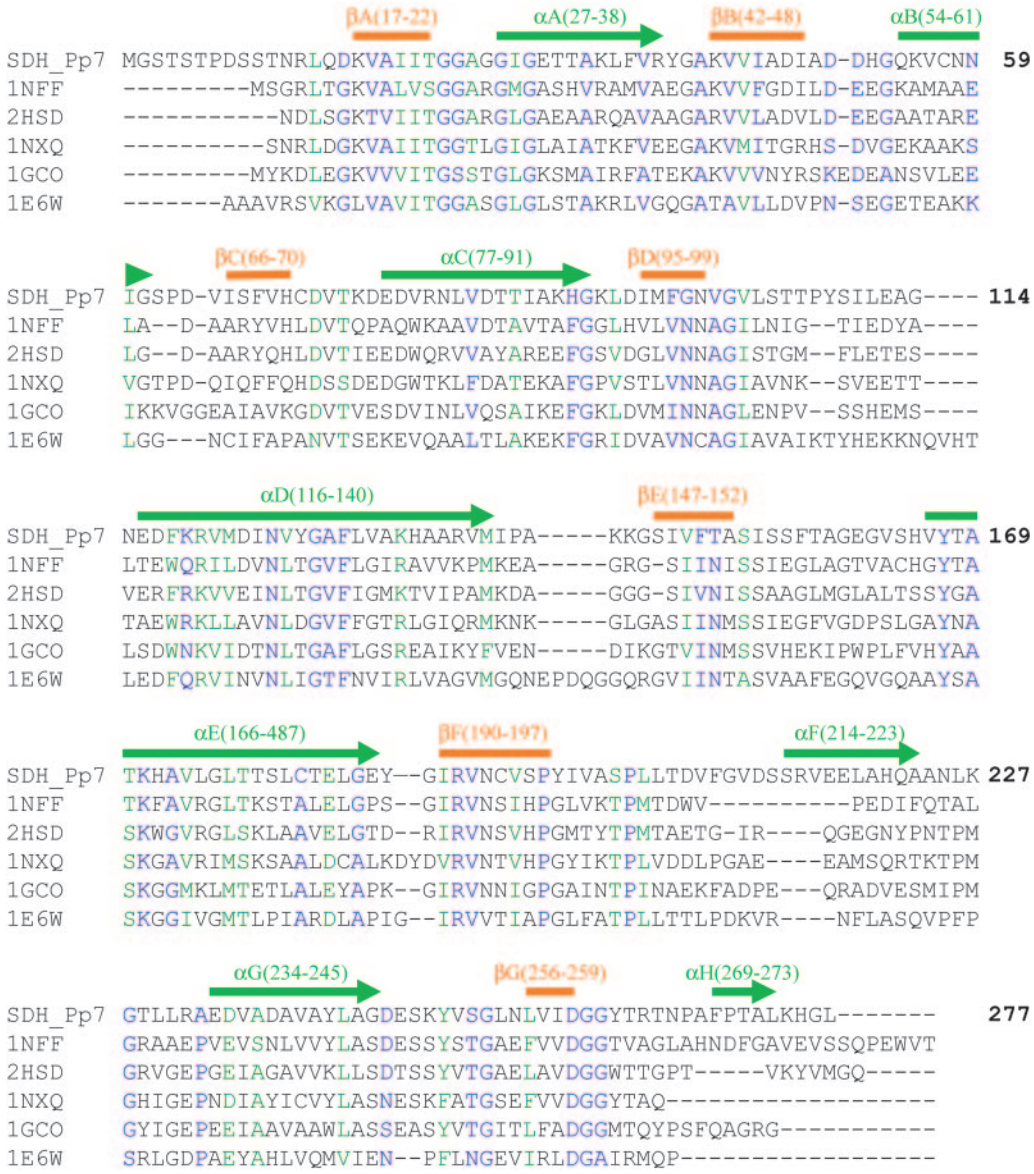

FIG. 5. **Amino acid sequence alignment comparison of SDH_Pp7, Rv2002 gene product from *M. tuberculosis* (PDB 1NFF), 3α,20-β-hydroxysteroid dehydrogenase from *S. exfoliatus* (PDB 2HSD), *R*-specific alcohol dehydrogenase from *L. brevis* (PDB 1NXQ), glucose dehydrogenase from *B. megaterium* (PDB 1GCO), and 3-hydroxyacyl-CoA dehydrogenase from rat brain (PDB 1E6W).** Secondary structural elements of SDH_Pp7 are highlighted in colored *bars*.

by a stacking interaction with the Pro[197], and its carbonyl oxygen is interacting with the backbone amide nitrogen of Val[200] (Fig. 6*B*). The side chains of two residues, Tyr[167] and Lys[171], of the catalytic triad are within hydrogen bonding distance of the nicotine amide ribose, O-2′ and O-3′, respectively, as shown (Fig. 6*B,* see *inset*), thereby possibly fixing the position of the nicotinamide ring during catalysis and only permitting hydride transfer for the substrate to take up the pro-*S*-hydride form in the conversion to NADH. Additionally, the phenolic group of Tyr[167] is located close (4.0 Å) to the C-4 atom of the nicotine amide ring, whereas the side chain of Asp[47] is within the hydrogen bonding distance to the O-3′ moiety of the adenine ribose and the N-3 atom of the adenine ring (Fig. 6*B*). As mentioned above, the small loop following βB that contains this Asp[47] residue and the adjacent αB thus becomes less flexible after NAD^+ is bound as reflected in the corresponding temperature factors (Fig. 7).

Like other typical SDRs, SDH_Pp7 has a glycine-rich motif, G*XX*G*XX*G, at the first β-α-β unit ([23]GGAGGIG[29]), which is known to participate in binding of the pyrophosphate group of NAD^+ through a helical dipole of αA. The pyrophosphate group of the NAD^+ in particular is within hydrogen bonding distance to the backbone amide nitrogen of residues Ile[28], thereby N-capping it and compensating for the helix macro-dipole (52). All the amino acids in this tight turn between βA and αB thus show relatively high temperature factors probably facilitating their interaction with NAD^+ via conformational flexibility. A preference for NADH over NADPH is achieved accordingly by charge repulsion resulting from the highly conserved Asp[47] in the pocket that is normally occupied by the 2′-phosphate group of NADPH (50). This acidic amino acid in βB, Asp[47], is often found in SDR enzymes that preferentially bind NAD(H), *i.e.* to form a hydrogen bond to both hydroxyl groups of the adenine ribose of NAD(H) (50). Significantly, all of the residues involved in NAD^+ binding are highly conserved among SDH and SDRs from various species.

Substrate Binding of SDH and Catalytic Mechanism—The exact conformation of the bound (−)-matairesinol (**1a**) product and NAD^+ molecules was clearly defined in the experimental electron density map (Fig. 9*B*). In the observed arrangement of

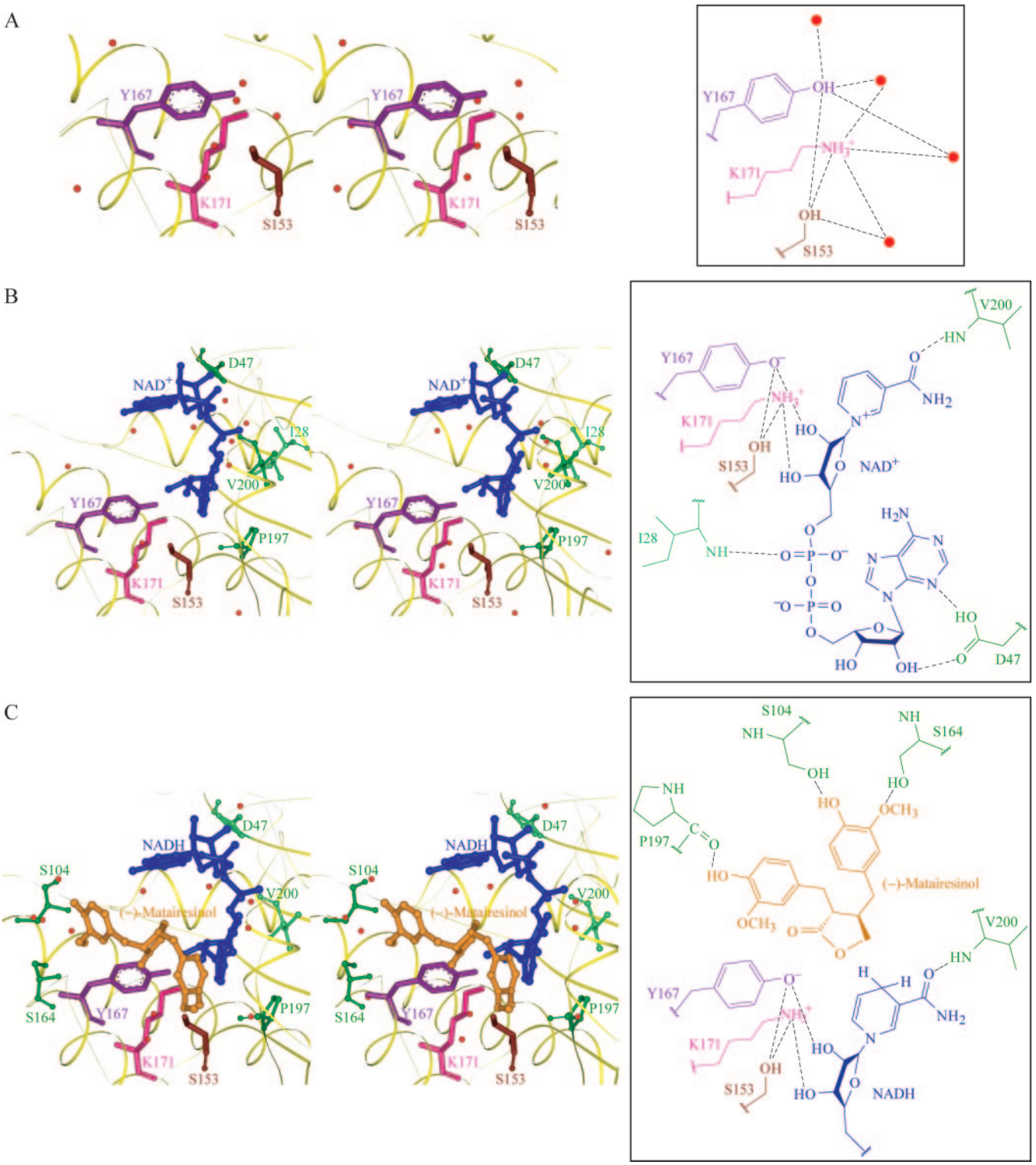

FIG. 6. **Structures of the substrate-binding pocket of SDH_Pp7 in apo-form and binary/ternary complexes.** *A*, apo-form: the catalytic triad residues Ser^{153} (*brown*), Tyr^{167} (*violet*), and Lys^{171} (*pink*) form a hydrogen bond network with each other and water molecules (shown as *red circles*). *B*, binary complex with bound NAD^+ (*blue*), where the latter has its nicotinamide ring in a *syn*-conformation and the adenine ring in an *anti*-conformation. The Tyr^{167} phenolic and Lys^{171}-protonated amino groups are hydrogen-bonded to 2′- and 3′-OH, respectively. *C*, ternary complex with NAD^+ (*blue*) and (−)-matairesinol (**1a**) (*light brown*).

the tetrameric form, a binding pocket for both the substrate and cofactor of the neighboring molecule in the asymmetric unit was located at positions similar to that of other SDR enzymes (Fig. 8*B*).

A deep groove containing the substrate-binding pocket is formed by three loops that connect βD and αD, βE and αE, and βF and αF, respectively, as well as the C-terminal helix (αH) of the adjacent subunit. In particular, the residues corresponding to one of these loops (200–213) and the αH (271–277) region have high temperature factors, with these potentially serving as a gate for the substrate and helping it to bind in the proper orientation (Fig. 7). In this way, the substrate-binding pocket is lined with hydrophobic residues, reflecting the nonpolar nature of the substrate. Both phenolic moieties of (−)-matairesinol

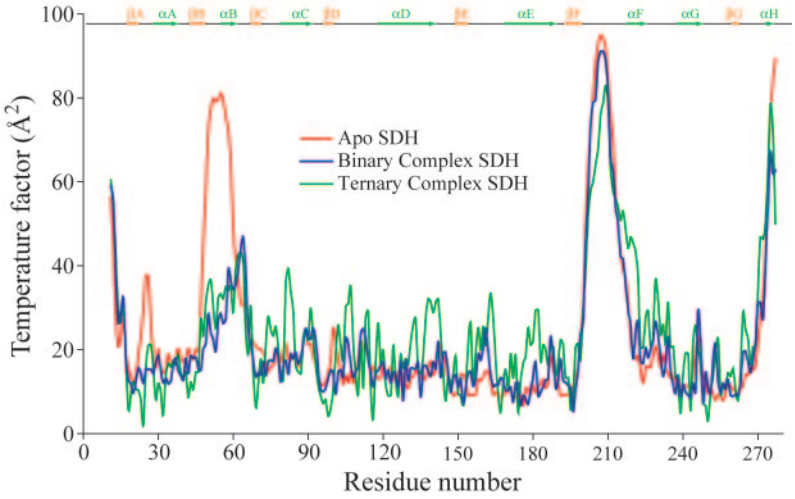

FIG. 7. **Backbone temperature factor plots of SDH_Pp7 crystal structures; apo-form (*red*) and binary (*blue*)/ternary (*green*) complexes.** Besides N- and C-terminal residues, the residues 201–215 and 272–277 show the temperature factors of their corresponding C-α atoms above 40 Å^2. In the two complex structures, the residues 48–61 have significantly lower temperature factors compared with that of the apo-form.

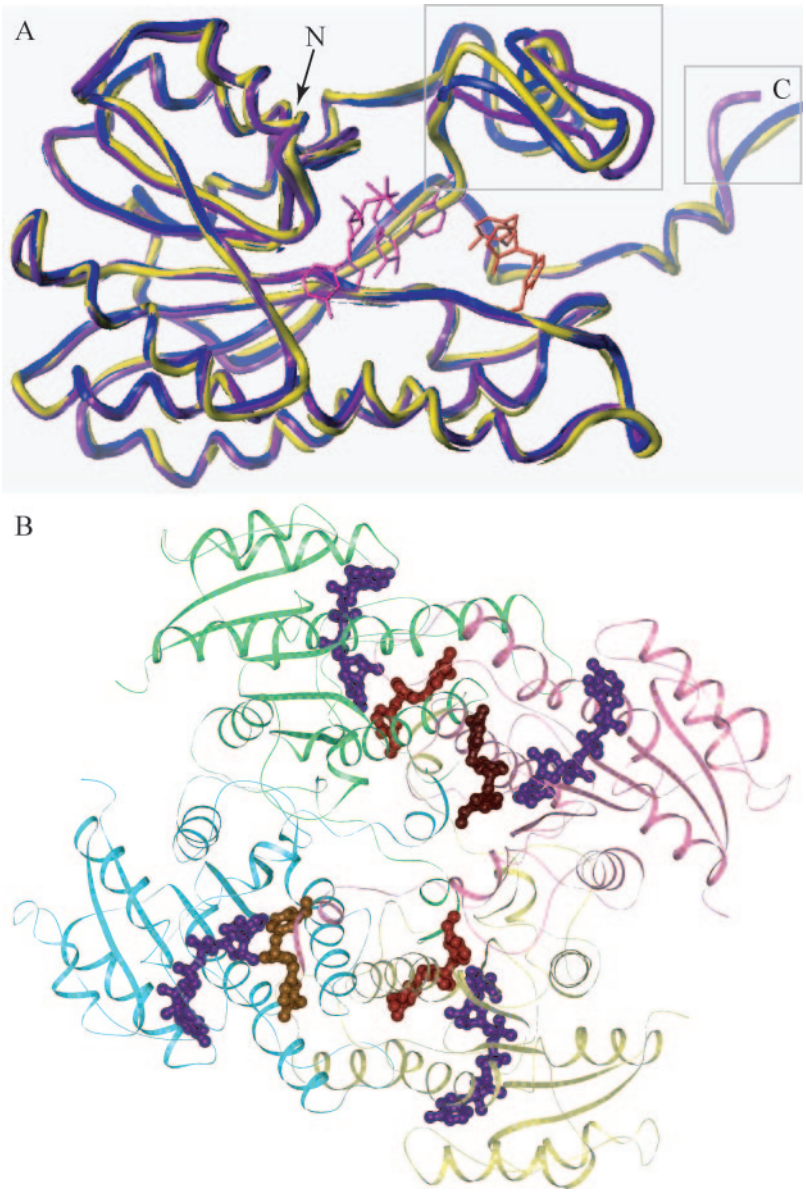

FIG. 8. **SDH complexes.** *A*, superimposed view of C-α positions of apo-form (*purple*), as well as binary (*yellow*) and ternary (*blue*) complexes of SDH_Pp7. Two areas of residues 201–222 and 272–277 show differences among structures. *B*, the position of NAD^+ and product in the SDH_Pp7 tetramer. In each case, NAD^+ and (−)-matairesinol (**1a**) are depicted in *violet* and *dark brown* colors, respectively.

(**1a**) and one of its methoxyl groups are surrounded by hydrophobic residues and anchored to the side-chain hydroxyl groups of Ser^{104} and Ser^{164} and the backbone of Pro^{197} through hydrogen bonds (Fig. 6*C*). The B-face of the nicotine amide ring is open to the cleft with the C-4 atom being ~5 Å from the target hydroxyl group of (−)-secoisolariciresinol (**2a**) (shown with (−)-

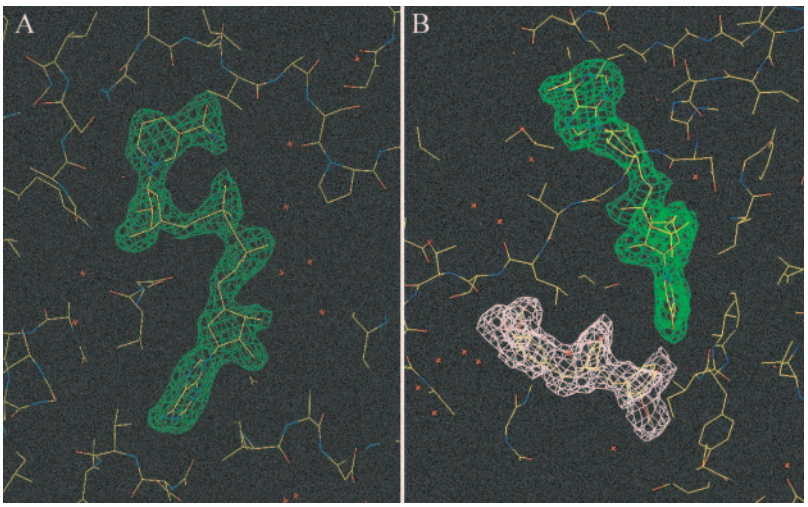

FIG. 9. **Difference ($F_o - F_c$) Fourier maps of binary (*A*) and ternary (*B*) complexes of SDH_Pp7.** NAD^+ and (−)-matairesinol (**1a**) have been modeled in this figure. The figures were prepared using Quanta (Accelrys).

matairesinol (**1a**) in Fig. 6*C*). Consequently, the nicotinamide and the substrate are in the proper orientation for the well established B-face-specific hydride transfer to C-4 from the corresponding substrate reaction center. This substrate-binding pocket also contains the conserved catalytic triad, Ser^{153}, Tyr^{167}, and Lys^{171}. Most interestingly, upon NAD^+ and substrate binding, no change was detected in either the conformation or the position of these amino acid residues.

The Lys^{171} residue lowers the pK_a of the phenolic hydroxyl group of the Tyr^{167} in the catalytic triad together with the positively charged NAD^+ (50, 53). The Ser^{153} residue then shares its proton with the phenolic anionic group of Tyr^{167} (Fig. 6*C*, *inset*), and in this way, the latter can serve as a general base in substrate deprotonation during catalysis (50, 53). Concomitant deprotonation of the (−)-secoisolariciresinol (**2a**) is then presumed to occur via the phenolic anion of Tyr^{167} with hydride transfer to NAD^+, followed by nucleophilic attack to form the (−)-lactol intermediate (**13a**) from (−)-secoisolariciresinol (**2a**). Subsequent dehydrogenation of the (−)-lactol (**13a**) can then occur by the same process involving Tyr^{167} as before and a newly bound NAD^+ molecule to afford the dibenzyl furanone, (−)-matairesinol (**1a**).

In this regard, only the one enantiomeric substrate, *i.e.* (−)-secoisolariciresinol (**2a**), was able to be modeled into this substrate-binding pocket using the same hydrogen bonds between the backbone and the two phenolic moieties observed in the quaternary (−)-matairesinol (**1a**) complex structure. In this modeled position, the target hydroxyl groups of the (−)-secoisolariciresinol (**2a**) are in the proper orientation and distance from the functional groups, but the corresponding hydroxyl groups of the stereoisomer, (+)-secoisolariciresinol (**2b**), cannot be fitted by using the same constraints of the hydrogen bonds; this in turn perhaps explains the enantiospecificity of SDH_Pp7.

Concluding Remarks—In planta, matairesinol (**1**) is a central precursor in the biosynthesis of numerous lignans, including the important antiviral and anticancer agent podophyllotoxin (6). In order to understand comprehensively the molecular basis of these multistep enzymatic reactions and the structure/function relationships of the participating enzymes, we are systematically characterizing all of the enzymes in the biochemical pathway to this "phytoestrogenic" lignan. We previously employed x-ray crystallography to determine the structure of the enantiospecific enzyme in the same biosynthetic pathway, *i.e.* the bifunctional NADPH-dependent PLRs (28), which converts pinoresinol (**11**) into lariciresinol (**12**) and then secoisolariciresinol (**2**). Based on detailed structural analyses and site-directed mutagenesis, the critical residues in the enzyme-active site of PLRs were determined, as well as that of the two evolutionarily related enzymes phenylcoumaran benzylic ether reductase and isoflavone reductase (28).

In this paper, we now report the crystal structure of the NAD(H)-dependent SDH, which catalyzes the next step, *i.e.* the enantiospecific conversion of (−)-secoisolariciresinol (**2a**) into (−)-matairesinol (**1a**). The enantiospecific SDH, however, differs markedly from the enantiospecific PLRs evolutionarily, because the crystal structure of SDH_Pp7 has an overall structure quite similar to members of the SDR family, many of which, due to their relation to tumor growth, have been very well studied (51). The continuously increasing members of this SDR family perform diverse functions in both prokaryotes and eukaryotes, and all appear to have the α/β single domain structure, *i.e.* including the dinucleotide-binding Rossmann fold and the homologous catalytic triad that contains a strictly conserved tyrosine residue. Most interestingly, despite their similar folding (α/β single domain structure) and catalytic mechanisms, the SDRs display very distinct substrate versatilities and can range from being rigid to flexible, from containing many polar groups to only a few, and from being large to small. Variation in the amino acid composition of the substrate-binding pocket is also well known for specificity of binding for various substrates, such as steroids, prostaglandins, sugars, and alcohols (51). As for many of the other SDR enzymes, the SDH_Pp7 is a tetramer both in solution and in the crystal lattice state and possesses a highly conserved catalytic triad, *i.e.* in this case, Ser^{153}, Tyr^{167}, and Lys^{171}. The triad is thus able to perform a concerted catalytic reaction in the conversion of (−)-secoisolariciresinol (**2a**) to (−)-matairesinol (**1a**).

Comprehensive understanding of the detailed reaction mechanisms of the participating enzymes in the (phytoestrogenic) lignan biosynthetic pathway thus continue to provide crucial insight into how this complex family of ubiquitous natural products (the lignans) (1, 54, 55) is formed in vascular plants. As we continue to add to our detailed knowledge of these enzymatic reactions, future work will be directed, for example, to metabolic engineering levels of both secoisolariciresinol (**2**) and matairesinol (**1**) in plant foodstuffs such as vegetables, grains, fruits, or as supplements for processed food items, *i.e.* in order to provide a facile source of these beneficial lignans in staple dietary foodstuffs for the benefits of humanity, or to provide an increased supply of the antiviral/anticancer lignans such as podophyllotoxin (**5**).

REFERENCES

1. Lewis, N. G., and Davin, L. B. (1999) in *Comprehensive Natural Products Chemistry* (Barton, Sir D. H. R., Nakanishi, K., and Meth-Cohn, O., eds) Vol. 1, pp. 639–712, Elsevier Science Ltd., London, UK

2. Davin, L. B., and Lewis, N. G. (2003) *Phytochem. Rev.* **2,** 257–288
3. Adlercreutz, H., Höckerstedt, K., Bannwart, C., Hämäläinen, E., Forsis, T., and Bloigu, S. (1988) *Prog. Cancer Res. Ther.* **35,** 409–412
4. Adlercreutz, H., Mousavi, Y., Clark, J., Höckerstedt, K., Hämäläinen, E., Wähälä, K., Mäkelä, T., and Hase, T. (1992) *J. Steroid Biochem. Mol. Biol.* **41,** 331–337
5. Xia, Z.-Q., Costa, M. A., Proctor, J., Davin, L. B., and Lewis, N. G. (2000) *Phytochemistry* **55,** 537–549
6. Canel, C., Moraes, R. M., Dayan, F. E., and Ferreira, D. (2000) *Phytochemistry* **54,** 115–120
7. Gardner, J. A. F., Barton, G. M., and MacLean, H. (1959) *Can. J. Chem.* **37,** 1703–1709
8. Gardner, J. A. F., MacDonald, B. F., and MacLean, H. (1960) *Can. J. Chem.* **38,** 2387–2394
9. Gardner, J. A. F., Swan, E. P., Sutherland, S. A., and MacLean, H. (1966) *Can. J. Chem.* **44,** 52–58
10. Fujita, M., Gang, D. R., Davin, L. B., and Lewis, N. G. (1999) *J. Biol. Chem.* **274,** 618–627
11. Gang, D. R., Fujita, M., Davin, L. B., and Lewis, N. G. (1998) *ACS Symp. Ser.* **697,** 389–421
12. Dinkova-Kostova, A. T., Gang, D. R., Davin, L. B., Bedgar, D. L., Chu, A., and Lewis, N. G. (1996) *J. Biol. Chem.* **271,** 29473–29482
13. Davin, L. B., Wang, H.-B., Crowell, A. L., Bedgar, D. L., Martin, D. M., Sarkanen, S., and Lewis, N. G. (1997) *Science* **275,** 362–366
14. Gang, D. R., Costa, M. A., Fujita, M., Dinkova-Kostova, A. T., Wang, H.-B., Burlat, V., Martin, W., Sarkanen, S., Davin, L. B., and Lewis, N. G. (1999) *Chem. Biol.* **6,** 143–151
15. Gang, D. R., Kasahara, H., Xia, Z.-Q., Vander Mijnsbrugge, K., Bauw, G., Boerjan, W., Van Montagu, M., Davin, L. B., and Lewis, N. G. (1999) *J. Biol. Chem.* **274,** 7516–7527
16. Ford, J. D., Davin, L. B., and Lewis, N. G. (1999) in *Plant Polyphenols 2: Chemistry, Biology, Pharmacology, and Ecology* (Hemingway, R. W., Gross, G. G., and Yoshida, T., eds) pp. 675–694, Kluwer Academic/Plenum Publishing Corp., New York
17. Davin, L. B., and Lewis, N. G. (2000) *Plant Physiol.* **123,** 453–461
18. Burlat, V., Kwon, M., Davin, L. B., and Lewis, N. G. (2001) *Phytochemistry* **57,** 883–897
19. Ford, J. D., Huang, K.-S., Wang, H.-B., Davin, L. B., and Lewis, N. G. (2001) *J. Nat. Prod.* **64,** 1388–1397
20. Ford, J. D. (2001) *Cancer Chemopreventive Flax Seed Lignans: Delineating the Metabolic Pathway(s) to the SDG-HMG Ester-linked Polymer.* Ph.D. thesis, Washington State University
21. Xia, Z.-Q., Costa, M. A., Pélissier, H. C., Davin, L. B., and Lewis, N. G. (2001) *J. Biol. Chem.* **276,** 12614–12623
22. Wang, C.-Z., Davin, L. B., and Lewis, N. G. (2001) *J. Chem. Soc. Chem. Commun.* 113–114
23. Halls, S. C., and Lewis, N. G. (2002) *Biochemistry* **41,** 9455–9461
24. Kim, M. K., Jeon, J.-H., Davin, L. B., and Lewis, N. G. (2002) *Phytochemistry* **61,** 311–322
25. Kim, M. K., Jeon, J.-H., Fujita, M., Davin, L. B., and Lewis, N. G. (2002) *Plant Mol. Biol.* **49,** 199–214
26. Cho, M.-H., Moinuddin, S. G. A., Helms, G. L., Hishiyama, S., Eichinger, D., Davin, L. B., and Lewis, N. G. (2003) *Proc. Natl. Acad. Sci. U. S. A.* **100,** 10641–10646
27. Davin, L. B., Wang, C.-Z., Helms, G. L., and Lewis, N. G. (2003) *Phytochemistry* **62,** 501–511
28. Min, T., Kasahara, H., Bedgar, D. L., Youn, B., Lawrence, P. K., Gang, D. R., Halls, S. C., Park, H., Hilsenbeck, J. L., Davin, L. B., Lewis, N. G., and Kang, C. (2003) *J. Biol. Chem.* **278,** 50714–50723
29. Moinuddin, S. G. A., Hishiyama, S., Cho, M.-H., Davin, L. B., and Lewis, N. G. (2003) *Org. Biomol. Chem.* **1,** 2307–2313
30. Teoh, K. H., Ford, J. D., Kim, M.-R., Davin, L. B., and Lewis, N. G. (2003) in *Flaxseed in Human Nutrition* (Thompson, L. U., and Cunnane, S. C., eds) 2nd Ed., pp. 41–62, AOCS Press, Champaign, IL
31. Halls, S. C., Davin, L. B., Kramer, D. M., and Lewis, N. G. (2004) *Biochemistry* **43,** 2587–2595
32. Ralph, J., MacKay, J. J., Hatfield, R. D., O'Malley, D. M., Whetten, R. W., and Sederoff, R. R. (1997) *Science* **277,** 235–239
33. Morreel, K., Ralph, J., Kim, H., Lu, F., Goeminne, G., Ralph, S., Messens, E., and Boerjan, W. (2004) *Plant Physiol.* **136,** 3537–3549
34. Morreel, K., Ralph, J., Lu, F., Goeminne, G., Busson, R., Herdewijn, P., Goeman, J. L., Van der Eycken, J., Boerjan, W., and Messens, E. (2004) *Plant Physiol.* **136,** 4023–4036
35. Ralph, J., Hatfield, R. D., Piquemal, J., Yahiaoui, N., Pean, M., Lapierre, C., and Boudet, A. M. (1998) *Proc. Natl. Acad. Sci., U. S. A.* **95,** 12803–12808
36. Anterola, A. M., and Lewis, N. G. (2002) *Phytochemistry* **61,** 221–294
37. Katayama, T., and Kado, Y. (1998) *J. Wood Sci.* **44,** 244–246
38. Umezawa, T. (2003) *Phytochem. Rev.* **2,** 371–390
39. Niemetz, R., and Gross, G. G. (2003) *Phytochemistry* **64,** 1197–1201
40. Niemetz, R., and Gross, G. G. (2003) *Phytochemistry* **62,** 301–306
41. Chu, A., Dinkova, A., Davin, L. B., Bedgar, D. L., and Lewis, N. G. (1993) *J. Biol. Chem.* **268,** 27026–27033
42. Ford, J. D., Davin, L. B., and Lewis, N. G. (2000) in *Proceedings of the 58th Flax Institute of the United States*, Fargo, ND, March 23–25, 2000 (Carter, J. F., ed) pp. 39–48, The Flax Institute, Fargo, ND
43. Suzuki, S., Umezawa, T., and Shimada, M. (1998) *Biosci. Biotechnol. Biochem.* **62,** 1468–1470
44. Umezawa, T., Davin, L. B., and Lewis, N. G. (1991) *J. Biol. Chem.* **266,** 10210–10217
45. Yang, J. K., Park, M. S., Waldo, G. S., and Suh, S. W. (2003) *Proc. Natl. Acad. Sci., U. S. A.* **100,** 455–460
46. Navaza, J. (1994) *Acta Crystallogr. Sect. A* **50,** 157–163
47. Brunger, A. T. (1992) *X-PLOR: A System for Crystallography and NMR,* Version 3.1. Yale University, New Haven
48. Holm, L., and Sander, C. (1993) *J. Mol. Biol.* **233,** 123–138
49. Altschul, S. F., Madden, T. L., Schäffer, A. A., Zhang, J., Zhang, Z., Miller, W., and Lipman, D. J. (1997) *Nucleic Acids Res.* **25,** 3389–3402
50. Powell, A. J., Read, J. A., Banfield, M. J., Gunn-Moore, F., Yan, S. D., Lustbader, J., Stern, A. R., Stern, D. M., and Brady, R. L. (2000) *J. Mol. Biol.* **303,** 311–327
51. Duax, W. L., Griffin, J. F., and Ghosh, D. (1996) *Curr. Opin. Struct. Biol.* **6,** 813–823
52. Barbosa Pereira, P. J., Macedo-Ribeiro, S., Párraga, A., Pérez-Luque, R., Cunningham, O., Darcy, K., Mantle, T. J., and Coll, M. (2001) *Nat. Struct. Biol.* **8,** 215–220
53. Breton, R., Housset, D., Mazza, C., and Fontecilla-Camps, J. C. (1996) *Structure (Lond.)* **4,** 905–915
54. Lewis, N. G., Kato, M. J., Lopes, N., and Davin, L. B. (1995) *ACS Symp. Ser.* **588,** 135–167
55. Lewis, N. G., and Davin, L. B. (1994) *ACS Symp. Ser.* **562,** 202–246